Applied Catalysis B: Environmental 142–143 (2013) 705–717

Contents lists available at SciVerse ScienceDirect

Applied Catalysis B: Environmental

journal homepage: www.elsevier.com/locate/apcatb

# Ceria added Sb-$V_2O_5$/$TiO_2$ catalysts for low temperature $NH_3$ SCR: Physico-chemical properties and catalytic activity

Kyung Ju Lee[a,b], Pullur Anil Kumar[b], Muhammad Salman Maqbool[b,c], Komateedi Narayana Rao[b], Kwang Ho Song[a], Heon Phil Ha[b,*]

[a] Department of Chemical and Biological Engineering, Korea University, Anam-dong Seongbuk-gu, Seoul, 136-701, Republic of Korea
[b] Center for Materials Architecturing, Korea Institute of Science and Technology, Cheongryang, Seoul, 130-650, Republic of Korea
[c] Department of Clean Energy and Chemical Engineering, University of Science and Technology, Daejon, 305-350, Republic of Korea

ARTICLE INFO

*Article history:*
Received 8 February 2013
Received in revised form 28 May 2013
Accepted 30 May 2013
Available online 7 June 2013

*Keywords:*
Sb-$V_2O_5$-Ce/$TiO_2$
Ceria effect
XPS
TPD
Brønsted acid sites

ABSTRACT

A systematic investigation of the effect of ceria loading over Sb-$V_2O_5$/$TiO_2$ catalysts was carried out for the selective catalytic reduction (SCR) of $NO_x$ by $NH_3$. The various ceria loaded Sb-$V_2O_5$/$TiO_2$ catalysts were prepared by deposition precipitation and impregnation methods. Addition of 10% ceria to Sb-$V_2O_5$/$TiO_2$ catalyst significantly enhanced the $NO_x$ conversion at wide temperature range of 220–500 °C. The 10% ceria loaded Sb-$V_2O_5$/$TiO_2$ catalyst showed superior $N_2$ selectivity (>95%) throughout the reaction temperatures. The physicochemical characteristics of the obtained catalysts were thoroughly characterized by BET surface area, X-ray diffractometry (XRD), temperature programmed desorption (TPD) of NO, $SO_2$ and $NH_3$, $H_2$- temperature programmed reduction (TPR), X-ray photoelectron spectroscopy (XPS) and in situ diffuse reflectance infrared Fourier transform spectroscopy (DRIFTS). The XRD results indicated the active components of antimony and vanadia were homogeneously dispersed over $CeO_2$/$TiO_2$. It was found that the addition of 10% ceria to Sb-$V_2O_5$/$TiO_2$ could enhance the total acidity and redox properties of the catalyst, which lead to show higher $NO_x$ conversions at wide temperature window. In XPS studies, increase in intensity of the chemisorbed mobile oxygen peak was observed for ceria loaded catalysts. In particular, the DRIFT spectra of ceria loaded Sb-$V_2O_5$/$TiO_2$ catalysts showed abundant Brønsted acid sites at 1436 and 1673 $cm^{-1}$ band, which are responsible for high $NO_x$ conversion. Furthermore, the results of NO and $SO_2$ TPD of 10% ceria loaded Sb-$V_2O_5$/$TiO_2$ catalyst showed enhancement of NO adsorption and $SO_2$ inhibition properties, which is thought to play a significant role in long term stability of the catalyst during $SO_2$ on–off study for 38 h at 240 °C.



## 1. Introduction

Over the past decades, nitrogen oxides (NO, $NO_2$ and $N_2O$) from the stationary and mobile sources have been remained as major air pollutants. They provoked a series of environmental issues, such as photochemical smog, acid rain, ozone depletion and greenhouse effects [1,2]. The removal of nitrogen oxides (NO) from stationary sources such as thermal power plants is mostly carried out by selective catalytic reduction (SCR) of NO using ammonia. In this course of study, ammonia-SCR catalysts have been extensively investigated for heavy-duty vehicles and industrial processes for the last 15–20 years [3–6]. Currently locomotive and marine diesel engines emit large amounts of NO containing emissions; these air pollutants are expected to grow due to the anticipated future growth in the use of diesel engines. In case of marine applications, typically high sulfur containing fuel was used; where limited research was attempted. As huge quantity of $SO_2$ contained emissions are occurred in these applications, it will not be allowed to use existing catalytic technologies. Environmental Protection Agency (EPA) regulations concerning NO emissions will become more stringent in the coming years. Recently, EPA mandated the Tier 4 regulation, which begins to take effect. Thus, many efforts are endeavored to meet the regulation. However, water vapor is one of the main components of NO containing exhaust and is frequently leads to deactivation of the catalysts. Moreover, there is still residual $SO_2$ remaining after the de-sulfurizer. Thus, $SO_2$ resistance needs to be considered. The ultimate goal will be to develop a low temperature active catalyst (LTC) for $NH_3$-SCR in the presence of excess $H_2O$ and $SO_2$, which is regarded as a challenging task over the world.

Most of the LTC have been investigated using $V_2O_5$, $Fe_2O_3$ and $MnO_x$ as active components on metal oxide supports such as $TiO_2$, $Al_2O_3$ and $ZrO_2$ [7–12]. The major roles of the supports are: (a) providing a huge surface area to separate the active phase and

* Corresponding author. Tel.: +82 29585461; fax: +82 29585599.
*E-mail addresses:* heonphil@kist.re.kr, heonphil@hanmail.net (H.P. Ha).

0926-3373/$ – see front matter © 2013 Elsevier B.V. All rights reserved.
http://dx.doi.org/10.1016/j.apcatb.2013.05.071

to prevent the chance of agglomeration; (b) furnishing the sufficiently large space for the catalytic reactions. It is known that the effective strategy to improve the sulfur tolerance was the use of titanium dioxide ($TiO_2$) as a supporting material [13]. Matsumoto et al. [14] reported that the decomposition temperature of sulfates on a $TiO_2$ support was lower than that of $Al_2O_3$ support under reducing conditions. In addition, it is also known that $CeO_2$ can promotes performance of various catalytic reactions such as $CO_2$ activation [15], CO oxidation [16] and CO/NO removal [17] owing to its unique abilities to shift electrons easily between reduced and oxidized states ($Ce^{3+} \leftrightarrow Ce^{4+}$) and to accommodate variable levels of bulk and surface oxygen vacancies [18,19]. Therefore, ceria can be expected to enhance the oxidization of NO to $NO_2$ and thereby increasing the NO reduction activity by ammonia. Thus, it is considered here to verify the effect of ceria on NO reduction over a series of $TiO_2$ based oxides.

Nowadays, the commercial catalysts used for SCR in industry are mainly based on $V_2O_5$–$WO_3$/$TiO_2$. Although the vanadia–titania based catalysts are highly active and quite resistant to $SO_2$, there are several drawbacks like: (a) poor $N_2$ selectivity at high temperatures due to $N_2O$ formation and direct $NH_3$ oxidation; (b) higher amount of toxic $V_2O_5$; (c) high conversion of $SO_2$ to $SO_3$; (d) the phase transformation of $TiO_2$ from anatase to rutile at high temperatures (above 500 °C); and (e) this catalyst is rather active within a narrow temperature window of 300–400 °C [20,21], while this temperature range also helps to avoid pore plugging from the deposition of ammonium sulfate salts such as $NH_4HSO_4$ and $(NH_4)_2SO_4$ on the catalyst surface. Many efforts have been tried by the researchers to modify the $V_2O_5$–$WO_3$/$TiO_2$ catalyst system for $NH_3$ SCR. Therefore, the present investigation was undertaken on the aforesaid background. Taking into consideration to improve the low temperature conversion, antimony-based catalysts are adopted for the title reaction. We have reported highly efficient $V_2O_5$/$TiO_2$ catalyst promoted by antimony [22] instead of using expensive $WO_3$. In the present study, extensive work has been carried out to further enhance catalytic properties of formerly developed catalyst by ceria loaded novel composite catalytic system. The synthesized catalysts were thoroughly characterized by X-ray diffraction (XRD), X-ray photoelectron spectroscopy (XPS), temperature programmed desorption (TPD) of NO, $SO_2$ and $NH_3$, $H_2$-TPR (temperature programmed reduction), BET (Brunauer–Emmett–Teller) surface area, transmission electron microscopy (TEM) and in situ diffuse reflectance infrared Fourier transform spectroscopy (DRIFTS).

## 2. Experimental

### 2.1. Catalyst preparation

The $V_2O_5$-Ce/$TiO_2$ and Sb-$V_2O_5$-Ce/$TiO_2$ catalysts were prepared by incipient wetness co-impregnation of vanadium and antimony on prepared $CeO_2$/$TiO_2$ support. Required quantity of ammoniummetavanadate ($NH_4VO_3$, Junsei, 99%) was added to the oxalic acid solution and heated to form ammonium oxalate solution. Separately, an aqueous solution of antimony acetate was prepared by using antimony acetate ($Sb(CH_3COO)_3$, Alfa Aesar, 99.99%). Both of these solutions were added to the beaker containing calculated amount of $CeO_2$/$TiO_2$ powder; after 30 min of vigorous stirring, the solution was dried in a rotary evaporator at 50 °C. The obtained powder catalyst was dehydrated over night at 120 °C and then calcined at 500 °C in air for 5 h.

The $CeO_2$/$TiO_2$ support was synthesized by deposition precipitation method by hydrolysis with ammonium hydroxide (Aldrich, 25%) [23]. In a typical experiment, the required quantities of cerium (III) nitrate ($Ce(NO_3)_3{\cdot}6H_2O$, Alfa Aesar, 99.5%) and commercial $TiO_2$ (DT-51, Millennium Chemicals) powders were mixed together in a beaker containing de-ionized water. To this mixture solution, dilute aqueous ammonia was added as a precipitating agent and the resultant precipitate was filtered off. The obtained cake was oven dried at 120 °C for 12 h and then calcined at 500 °C for 5 h. The mole ratio of Sb/V (2 wt% Sb and 2 wt% V) was maintained same as 1:1 in all the prepared catalysts. The obtained $V_2O_5$-Ce/$TiO_2$ and Sb-$V_2O_5$-Ce/$TiO_2$ catalysts were denoted as V*x*Ce/$TiO_2$ and SbV*x*Ce/$TiO_2$ (*x* = 0, 5, 10 and 20 wt% of ceria).

### 2.2. Characterization techniques

The catalysts were analyzed by powder XRD (Bruker) and the spectra were recorded using Ni-filtered Cu $K_\alpha$ radiation operated at 40 kV and 20 mA. The BET (Brunauer–Emmett–Teller) surface area was measured from the $N_2$ adsorption and desorption isotherms at −196 °C using the ASAP-2010 (Micromeritics) analyzer. TEM analysis (Transmission electron microscopy) was performed on a JEM 2100F (JEOL Co.) electron microscope equipped with EDS (energy dispersive X-ray spectroscopy) operating at an acceleration voltage of 200 kV and 2 Å point-to-point resolution. Catalysts were supported on a copper grid by dropping ethanol suspensions containing uniformly dispersed powders. NO, $SO_2$ and $NH_3$ TPD experiments were carried out using the AutoChem II-2920 (Micromeritics) chemisorptions analyzer. For each experiment, 100 mg of catalyst was placed in a U-shaped quartz cell and preconditioned at 400 °C in 10% $O_2$/He gas at a flow rate of 50 mL $min^{-1}$ and then purged with He gas. For $NH_3$, NO and $SO_2$ TPD, 5% $NH_3$, 1% NO and 1% $SO_2$ under He balance were used as adsorption media in 50 mL $min^{-1}$ flow at 50 °C for 60 min, respectively. Furthermore, the samples were purged with He gas to remove the physically adsorbed gases at the same temperature. Afterwards, the TPD run was conducted from 50 to 900 °C at a heating rate of 10 °C $min^{-1}$. Simultaneously, NO-TPD-Mass spectra were analyzed by HPR-20 QIC (Quartz Inert Capillary) (HIDEN analytical) real time gas analyzer (RGA) for multiple species molecular weight up to 300 amu. The quantity of $NH_3$ ($NH_3$-TPD) was calculated by measuring the average area of the 5 consecutive 1 cc volume pulse injections (similar areas) of 5% $NH_3$/He gas. $H_2$-TPR experiments were carried out by heating the catalysts (each 100 mg) at a linear heating rate of 10 °C $min^{-1}$ between 50 and 1000 °C with 10% $H_2$/Ar at a constant flow rate of 50 mL $min^{-1}$. XPS studies were carried out by using PHI 5800 ESCA system, employing a non–monochromatic Al $K_\alpha$ (1486.6 eV) source. The binding energies were referenced to the C 1s line at 284.6 eV from adventitious carbon.

### 2.3. Activity measurements

The SCR of $NO_x$ ($NO + NO_2$) over the synthesized catalytic materials was evaluated by using ammonia as a reductant. The conversion of $NO_x$ was determined over a down flow fixed-bed reactor system. The quartz reactor (1 cm o.d. and 50 cm length) was placed vertically in a tubular furnace connected to a temperature controller indicator. To minimize the mass transfer limitations, the catalyst was sieved with 40–50 mesh size and then charged into the quartz reactor using quartz wool. Prior to each experiment, about 0.5 mL catalyst was pre-treated by a mixture of 3% $O_2$ and $N_2$ flowing at 500 °C for 1 h. A reaction stream consisting of 800 ppm $NO_x$, 800 ppm $NH_3$, 3 vol% $O_2$, 6 vol% $H_2O$, 800 ppm $SO_2$ and $N_2$ balance was fed into the reactor system through mass flow controllers with a total flow rate of 500 mL $min^{-1}$ and at a space velocity of 60,000 $h^{-1}$. Water vapor was produced by passing $N_2$ gas through a heated glass wash bottle containing de-ionized water. Catalytic activity measurements were performed in the temperature range between 180 and 500 °C (carried with and without $SO_2$ and $H_2O$). The effluent from the reactor was analyzed by an online NDIR Fuji

NO and $SO_2$ analyzer. $NO_2$ amount was determined by converting $NO_2$ into NO with Gas converter series CG-2M analyzer. The ammonia concentration was measured before ($[NH_3]_{in}$) and after ($[NH_3]_{out}$) the reaction by the GASTEC (Model GV-100) detector. Varian Micro GC equipped with a TCD (thermal conductivity detector) was used to detect $N_2$ and $N_2O$. Poraplot Q and Molecular Sieve 5A columns were used to monitor $N_2O$ and $N_2$, respectively. The percentage conversions of $NO_x$, $NH_3$ and selectivities of $N_2$ and $N_2O$ were calculated by using the formulae given below.

$$NO_x\text{conversion} = ([NO_x]_{in} - [NO_x]_{out})/[NO_x]_{in} \times 100 \quad (1)$$

$$NH_3\text{conversion} = ([NH_3]_{in} - [NH_3]_{out})/[NH_3]_{in} \times 100 \quad (2)$$

$$N_2O\text{selectivity} = 2 \times [N_2O]/([NO_x]_{in} + [NH_3]_{in} - [NO_x]_{out} - [NH_3]_{out}) \times 100 \quad (3)$$

$$N_2\text{selectivity} = \{[NO_x]_{in} + [NH_3]_{in} - [NO_x]_{out} - [NH_3]_{out} - [NO_2]_{out} - 2 \times [N_2O]_{out}\}/\{[NO_x]_{in} + [NH_3]_{in} - [NO_x]_{out} - [NH_3]_{out}\} \times 100 \quad (4)$$

where $[NO_x]_{in}$ and $[NO_x]_{out}$ are the initial (inlet) and final (outlet) concentrations of $NO_x$.

### 2.4. In situ DRIFTS experiments

In situ DRIFT spectra were recorded by the JASCO (FT/IR-4200) Fourier transform infrared spectrometer, equipped with an in situ diffuse reflection chamber and a high sensitivity MCT/A detector cooled by liquid nitrogen. DRIFT spectra were recorded by accumulating 50 scans at a resolution of 4 $cm^{-1}$. Finely powdered catalyst was loaded in a porous alumina crucible and placed in a DRIFTS cell, equipped with KBr windows. Prior to each experiment, 20 mg of catalyst was heated in a high temperature DRIFTS cell at a rate of 10 °C $min^{-1}$ from room temperature to 400 °C under $N_2$ gas flow for 30 min, and then cooled to room temperature. For ammonia adsorption at room temperature, 2000 ppm of $NH_3$ was introduced into the DRIFTS cell for 30 min and then followed by purging with $N_2$ at 50, 150, 250 and 350 °C temperatures for 30 min. Transient in situ DRIFTS experiments were carried out by $NH_3$ (800 ppm) adsorption at 200 °C for 30 min, followed by purging with $N_2$ gas. NO (800 ppm) + 3% $O_2$ gas was then introduced into the DRIFTS cell at 200 °C, and spectra were recorded as a function of time.

## 3. Results and discussion

### 3.1. Activity studies

The effect of ceria over $SbV/TiO_2$ catalysts for $NO_x$ reduction by $NH_3$ was evaluated in terms of $NO_x$ conversion. The $NO_x$ conversion of $SbVxCe/TiO_2$ catalysts in the absence of $H_2O$ and $SO_2$ were shown in Fig. 1. It has been observed that the ceria loading over $SbV/TiO_2$ sample influenced the $NO_x$ reduction activity. The addition of ceria noticeably expanded the active temperature window for SCR reaction and also improved the $NO_x$ conversion. This improvement in $NO_x$ conversion was observed with the addition of ceria until 10 wt% and then decreased slightly, it could be due to the monolayer coverage of vanadia on 10 wt% ceria added catalyst (Fig. 1). It is well reported in the literature that vanadia loading in monolayer and sub monolayer surface coverage, are far more active than crystalline vanadia nanoparticles and the structure of $VO_x$ strongly influenced by the reducible oxides (e.g., ceria) [24]. Among all the

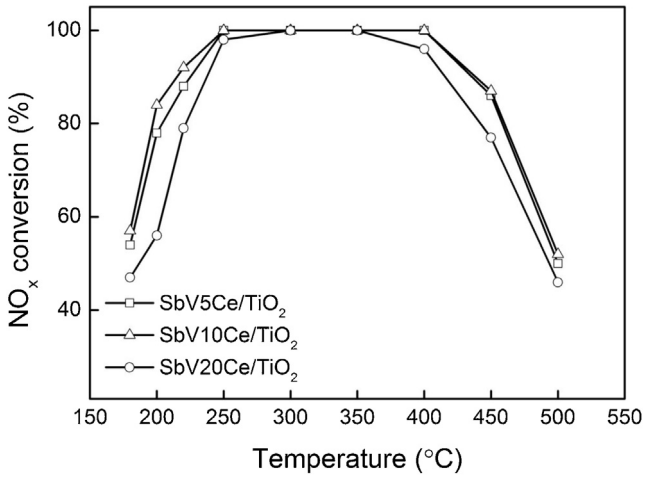


**Fig. 1.** $NO_x$ conversion of $SbV/TiO_2$ and ceria loaded $SbV/TiO_2$ samples calcined at 500 °C: Without $H_2O$ and $SO_2$. (Reaction conditions: $[NO_x] = [NH_3] = 800$ ppm, $[O_2] = 3$ vol%, $N_2$ balance, GHSV = 60,000 $h^{-1}$).

catalysts tested, $SbV10Ce/TiO_2$ catalyst exhibited the best performance with nearly higher than 90% of $NO_x$ conversion over a wide range of temperatures from 220 to 450 °C. Above 450 °C, the catalytic activity of all the samples was decreased due to the direct oxidation of ammonia [25]. For the purpose of industrial applications, it is very important to investigate the effect of $H_2O$ and $SO_2$ on SCR activities, which generally exists in exhaust and flue gas. In this regard, the effect of $H_2O$ and $SO_2$ were examined and the results are given in Fig. 2. With the addition of $H_2O$ and $SO_2$ into the reaction gas, the activity of $SbVxCe/TiO_2$ catalyst was slightly decreased, particularly at low temperatures. In the presence of $H_2O$ and $SO_2$, the $NO_x$ conversion over $SbV20Ce/TiO_2$ decreased to 68% from 79% whereas $SbV10Ce/TiO_2$ showed slight decrease to 90% from 92% at 220 °C. These results reveal that $SbV10Ce/TiO_2$ catalyst exhibits higher resistance against $H_2O$ and $SO_2$ than $SbV20Ce/TiO_2$ catalyst. At the same time, the $NO_x$ conversion was maintained higher than 85% in the temperature range of 220–500 °C. These results indicate that the addition of ceria enhanced the ability to resist $SO_2$ and $H_2O$ and promoted the $NO_x$ conversion at low and high temperature regions as well.

The $NO_x$ conversion activity comparison between $SbV/TiO_2$, $SbV10Ce/TiO_2$ and $V10Ce/TiO_2$ catalysts are shown in Fig. 3 without

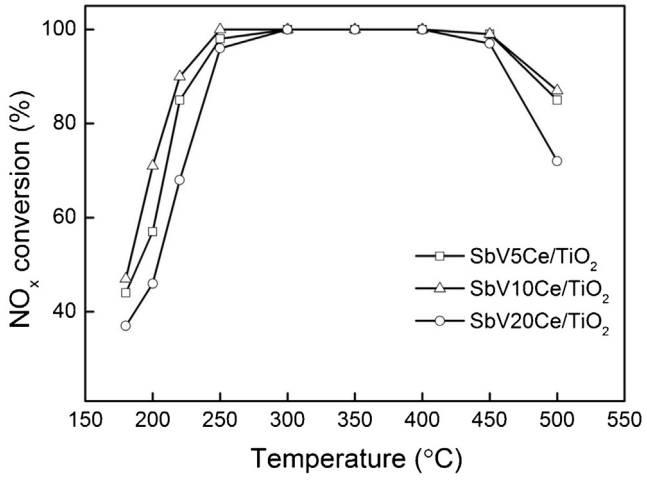


**Fig. 2.** $NO_x$ conversion of $SbV/TiO_2$ and ceria loaded $SbV/TiO_2$ samples calcined at 500 °C: With $H_2O$ and $SO_2$. (Reaction conditions: $[NO_x] = [NH_3] = 800$ ppm, $[O_2] = 3$ vol%, $H_2O = 6$ vol%, $SO_2 = 800$ ppm, $N_2$ balance, GHSV = 60,000 $h^{-1}$).

$H_2O$ and $SO_2$. Fig. 3 indicates that low and high temperature SCR activities were greatly enhanced with the addition of ceria. The $SbV/TiO_2$ catalyst with 10% ceria loading ($SbV10Ce/TiO_2$) showed the highest $NO_x$ conversions over a wide range of temperatures and best catalytic activity as compared to those of $SbV/TiO_2$ and $V10Ce/TiO_2$ catalysts. It can be clearly seen from the Fig. 3 that the $NO_x$ conversion over $SbV/TiO_2$ catalyst was noticeably decreased at above 400 °C due to direct oxidation of ammonia at high temperatures. However, the $NO_x$ conversion was retained higher than 85% over $SbV10Ce/TiO_2$ and $V10Ce/TiO_2$ catalysts until 450 °C temperatures. This seems that the addition of ceria retarded the direct oxidation of ammonia at high temperature region.

The effect of $H_2O$ and $SO_2$ on various catalysts at a space velocity of 60,000 $h^{-1}$ is displayed in Fig. 4. $NO_x$ and $NH_3$ conversions of $SbV/TiO_2$, $SbV10Ce/TiO_2$ and $V10Ce/TiO_2$ catalysts are shown in Fig. 4(A) and (B) as a function of temperature. At the operating temperatures below 250 °C, it is observed that the addition of 6 vol% $H_2O$ and 800 ppm $SO_2$ into the reaction stream reduced the catalytic activity, while above 350 °C higher $NO_x$ conversions were noticed [26]. These results suggest that water vapor and $SO_2$ had inhibition effect at lower temperatures. When the temperature is high, the catalysts show strong resistance to $H_2O$ and $SO_2$ [27]. It has been observed from the Fig. 4, the $SbV/TiO_2$ catalyst showed

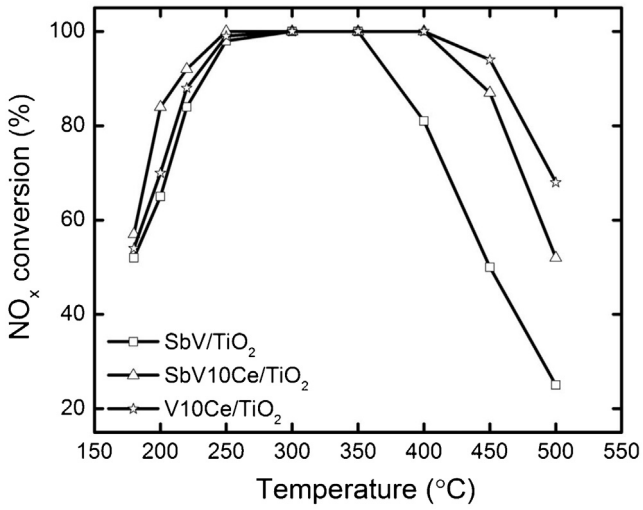


**Fig. 3.** $NO_x$ conversion vs Temperature on $SbV/TiO_2$, $SbV10Ce/TiO_2$ and $V10Ce/TiO_2$ samples calcined at 500 °C: Without $H_2O$ and $SO_2$. (Reaction conditions: $[NO_x] = [NH_3] = 800$ ppm, $[O_2] = 3$ vol%, $N_2$ balance, GHSV = 60,000 $h^{-1}$).

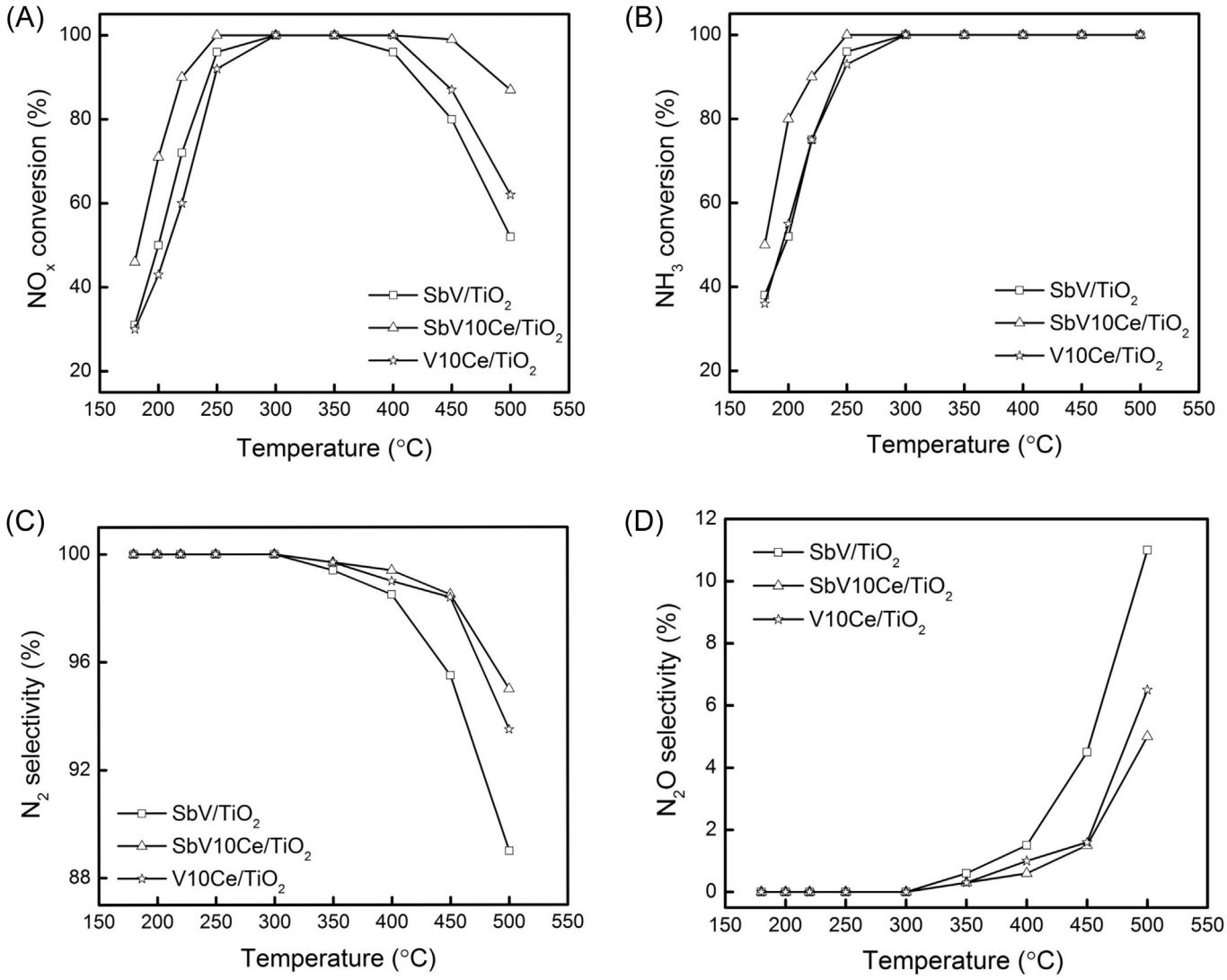


**Fig. 4.** Activity of $SbV/TiO_2$, $SbV10Ce/TiO_2$ and $V10Ce/TiO_2$ samples calcined at 500 °C under $H_2O$ and $SO_2$ (A) $NO_x$ conversion (B) $NH_3$ conversion (C) $N_2$ selectivity and (D) $N_2O$ selectivity. (Reaction conditions: $[NO_x] = [NH_3] = 800$ ppm, $[O_2] = 3$ vol%, $H_2O = 6$ vol%, $SO_2 = 800$ ppm, $N_2$ balance, GHSV = 60,000 $h^{-1}$).

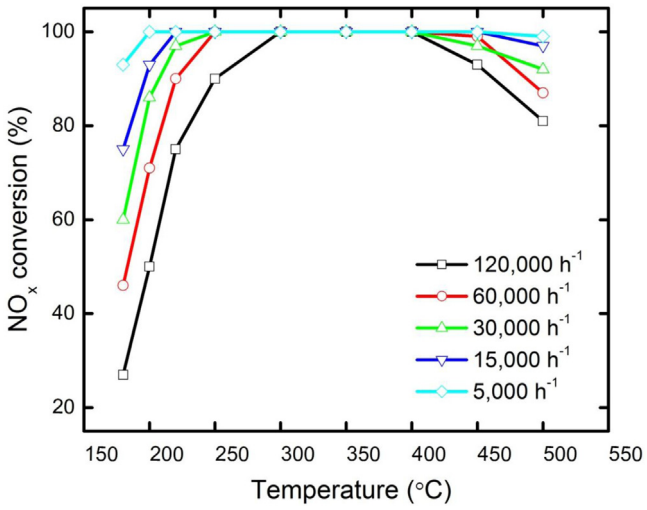


**Fig. 5.** $NO_x$ conversion as a function of GHSV for SbV10Ce/$TiO_2$ catalyst. (Reaction Conditions: $[NO_x] = [NH_3] = 800$ ppm, $[O_2] = 3$ vol%, $H_2O = 6$ vol%, $SO_2 = 800$ ppm, $N_2$ balance).

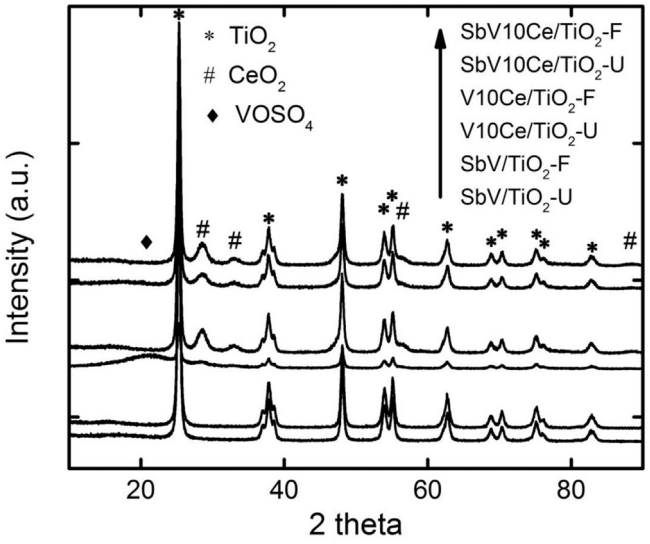


**Fig. 6.** XRD profiles of SbV/$TiO_2$, SbV10Ce/$TiO_2$ and V10Ce/$TiO_2$ fresh (F) and used (U) samples.

lower $NO_x$ conversions than the other two catalysts. However, the SbV10Ce/$TiO_2$ catalyst showed superior catalytic activity higher than 87% of $NO_x$ conversion in a wide temperature window from 220 to 500 °C. Once again the results revealed the addition of ceria could enhance the $SO_2$ and $H_2O$ resistance and reduced the direct oxidation of $NH_3$. As shown in Fig. 4 (B), the $NH_3$ slip was decreased significantly when 10% ceria was added to SbV/$TiO_2$ and achieved high $NH_3$ conversions than SbV/$TiO_2$ and V10Ce/$TiO_2$ catalysts. Therefore, the addition of ceria increased the activation of ammonia at low temperatures which lead to higher $NO_x$ conversions for SbV10Ce/$TiO_2$ catalysts even at low temperatures. The selectivities of $N_2$ and $N_2O$ over SbV/$TiO_2$, SbV10Ce/$TiO_2$ and V10Ce/$TiO_2$ catalysts are shown in Fig. 4(C) and (D), respectively. We have found that the formation of $N_2O$ started and accordingly the formation of $N_2$ was decreased above 300 °C. The $N_2O$ formation over SbV/$TiO_2$ catalyst increases at temperatures more than 350 °C and reaches a maximum of 11% at 500 °C. $N_2O$ is a major greenhouse gas and air pollutant and the impact of $N_2O$ on warming the atmosphere is over 300 times stronger than that of $CO_2$ (per unit weight) [28]. On the contrary, the decrease of $N_2O$ formation was observed with the addition of ceria to SbV/$TiO_2$ catalyst and showed an excellent $N_2$ selectivity over SbV10Ce/$TiO_2$ compared to SbV/$TiO_2$ and V10Ce/$TiO_2$ catalysts. It is worth noting that the SbV10Ce/$TiO_2$ catalyst show high $N_2$ selectivity more than 95% until the temperature as high as 500 °C. Among all the three catalysts, SbV10Ce/$TiO_2$ has the best $NO_x$ conversion and high $N_2$ selectivity in a wide temperature range of 220 to 500 °C. The addition of ceria improved the dispersion of antimony and vanadia over $TiO_2$ surface of the catalyst, which leads to excellent structural characteristics that is beneficial for the $NO_x$ reduction with ammonia [29,30].

Gas hourly space velocity (GHSV) is a very important factor to be considered in designing of the catalyst. Therefore, the influence of GHSV on the $NO_x$ conversions over SbV10Ce/$TiO_2$ catalyst has been investigated and is shown in Fig. 5. These activities are investigated at different space velocities from 5000 to 120,000 $h^{-1}$. It can be observed that the $NO_x$ conversion efficiency decreases rapidly with increasing space velocity, especially at low temperatures. However, the difference in $NO_x$ conversions becomes narrower at higher temperatures. It can be noticed from the results that complete $NO_x$ conversion was achieved at lowest temperatures around 200 °C at a space velocity of 5000 $h^{-1}$ and simultaneously widened the active temperature window. Although, the active temperature window at higher space velocities is slightly narrower than at the lower space velocities, the high temperature $NO_x$ conversion was maintained to be higher than 80% (>400 °C).

### 3.2. Catalytic characterization

Fig. 6 showed the X-ray diffractograms of various catalysts calcined at 500 °C. The XRD pattern of all the samples demonstrates standard $TiO_2$ anatase peaks [PDF-ICDD 86-1157]. In addition, the ceria promoted samples showed cubic ceria peaks at $2\theta = 28.5°$, 33.07°, 56.3° [PDF-ICDD 81-0792] [23]. The ceria based catalysts showed broader peaks compared to SbV/$TiO_2$ catalyst, which could be assigned to the small crystallites nature of the formed solids. No peaks due to solid solution between $TiO_2$ and $CeO_2$ were detected. Because of nominal addition of 2 wt% V and 2 wt% Sb, the peaks pertaining to these metal oxides were also not detected. Chiang et al. [31] have found that Sb/V mole ratio of 1, the characterization results of their work by XRD revealed that no crystalline $V_2O_5$ phase is present. Similarly, Sb/V ratio was maintained as 1 in our SbV/$TiO_2$ and SbV10Ce/$TiO_2$ catalysts. Therefore, the XRD results showed no peaks pertaining to vanadia and antimony due to well dispersion of these species on the surface of the support. In order to know the thermal stability of the materials at reaction conditions, the XRD patterns for used catalysts were analyzed. The used catalysts showed similar XRD patterns as like fresh catalysts, which may suggest the existence of small crystallites in used catalysts signifying the good thermal stability of the catalysts. In general, at high temperatures, pure $TiO_2$ may undergoes a phase transformation from anatase to rutile which usually begins above 500 °C [32,33]. Further, no such transformation or extra lines were noticed in the results. However, in case of V10Ce/$TiO_2$ catalyst XRD pattern, the broad peak at $2\theta = 21°$ was observed, which is assigned to the formation of $VOSO_4$ [PDF-ICDD 30-1431]. This could be formed due to the sulfation of vanadia by $SO_2$ gas under the reaction conditions. In our previous report on Sb promoted $V_2O_5/TiO_2$ [22], the quantum chemical calculation results revealed that the bonding strength between Sb and O, O (vanadia) and H of ammonium bisulfate becomes weak which led to an easy desorption of ammonium bisulfate. The XPS results of used catalyst also confirmed the less amount of formation of ammonium bisulfates on Sb promoted $V_2O_5/TiO_2$ compared to that on commercial catalyst. Hence, the presence of antimony caused the less formation of $VOSO_4$ on used catalysts of SbV/$TiO_2$ and SbV10Ce/$TiO_2$, which might be very small

**Table 1**
BET-SA $H_2$-TPR and $NH_3$-TPD results of the catalysts.

| Catalyst | BET-SA ($m^2$/g) | $H_2$-TPR | | $NH_3$-TPD |
|---|---|---|---|---|
| | | $T_{max}$ (°C) | $H_2$-uptake (μmol/$m^2$) | Total acidity (mmol/$m^2$) |
| $SbV/TiO_2$ | 71 | 464 | 1.18 | 0.57 |
| $V10Ce/TiO_2$ | 69 | 483 | 1.13 | 0.69 |
| $SbV10Ce/TiO_2$ | 73 | 488 | 1.76 | 0.78 |

$T_{max}$: Maximum peak temperature.

amount to the detection levels of XRD. Table 1 shows the results of BET surface area of the freshly prepared catalysts calcined at 500 °C. As seen from Table 1, the addition of ceria has some enhancement of surface area. However, all the synthesized catalysts showed moderate specific surface area around 70 $m^2g^{-1}$.

The NO-TPD patterns of the $SbV10Ce/TiO_2$, $V10Ce/TiO_2$ and $SbV/TiO_2$ catalysts calcined at 500 °C are showed in Fig. 7(A). Each catalyst pattern mainly consisted of three peaks. The first peak observed at low temperatures below 400 °C is consisted of two peaks appeared at 160 °C with a shoulder peak at above 250 °C. The second small is centered between 450 to 600 °C and the third one is much more intensive than the other two peaks and was appeared at temperature higher than 600 °C. While, the third peak on $Sb/TiO_2$ catalyst was shifted to low temperatures (<600 °C). As seen from Fig. 7(A), the intensity of the peak observed below 400 °C is very high for $SbV10Ce/TiO_2$ catalyst followed by $V10Ce/TiO_2$ and $SbV/TiO_2$. In order to identify the nature of these surface desorbed species the mass spectra (NO-TPD-MS) were recorded for the three catalysts. Fig. 7(B) and (C) depicts the mass spectra of NO and $O_2$. Apart from desorption of nitric oxide and oxygen also emission of $N_2$, $N_2O$, $NO_2$ and $H_2O$ was detected. Fig. 7(B) displayed the patterns obtained for $SbV10Ce/TiO_2$, $V10Ce/TiO_2$ and $SbV/TiO_2$ catalysts of NO mass signals. The NO desorption of $SbV/TiO_2$ catalyst showed single reduction peak at 270 °C and a small reduction at very high temperatures around 685 °C. However, the adsorption of NO increased with the addition of ceria to $V/TiO_2$, and attributed three peaks, first one is observed at 150 °C, second one at 250 °C, third one at 320 °C and very small peak at high temperatures at around 730 °C. Furthermore, the addition of ceria to $SbV/TiO_2$, the NO adsorption was drastically increased and showed desorption peak from 80 to 420 °C, followed by a small desorption peak at high temperatures around 730 °C. The NO peak observed at low

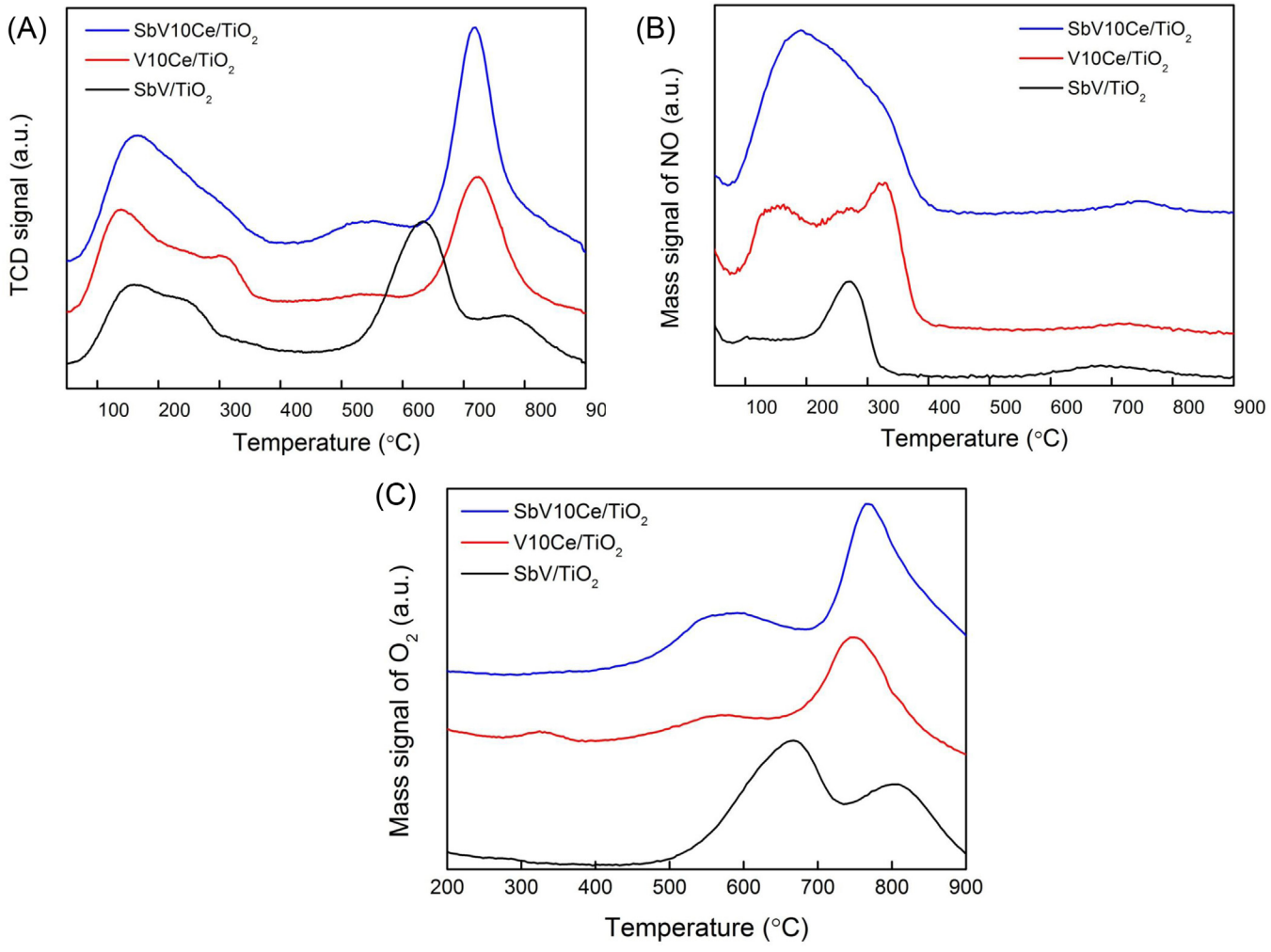


**Fig. 7.** NO-TPD-MS patterns of $SbV/TiO_2$, $SbV10Ce/TiO_2$ and $V10Ce/TiO_2$ samples (A) NO-TPD, (B) NO-Mass spectra and (C) $O_2$-Mass spectra.

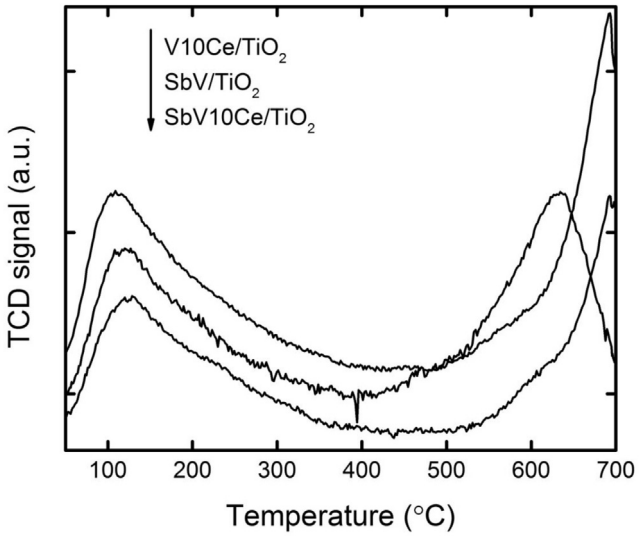


**Fig. 8.** $SO_2$-TPD patterns of $SbV/TiO_2$, $SbV10Ce/TiO_2$ and $V10Ce/TiO_2$ samples.

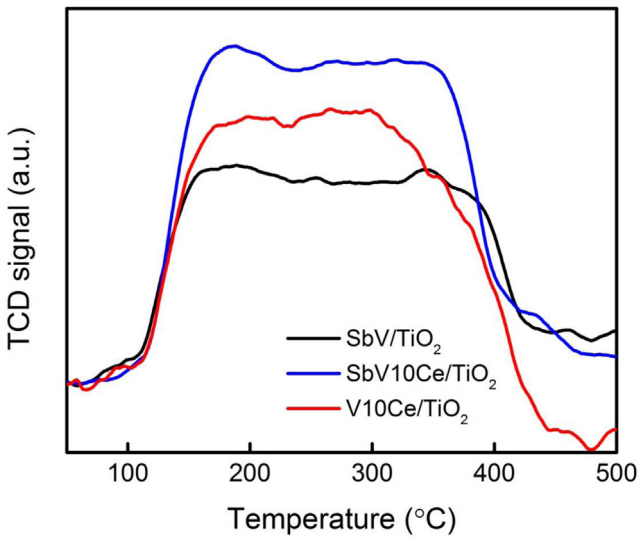


**Fig. 9.** $NH_3$-TPD patterns of $SbV/TiO_2$, $SbV10Ce/TiO_2$ and $V10Ce/TIO_2$ samples.

temperatures below 150 °C are attributed to weakly adsorbed NO species, the peak observed at 150–250 °C are attributed to medium and above 250–420 °C peak attributed to strongly adsorbed NO species. A small peak observed on all the three catalysts at the temperatures higher than 600 °C temperatures was attributed to the strongly chemisorbed NO species. Among all the catalysts, the addition of ceria to $SbV/TiO_2$ increased the adsorption properties of NO and as well as increased the desorption temperatures from low to high temperatures, which may led to show higher $NO_x$ conversions at wide temperatures. However, the mass signal corresponding to $N_2$, $N_2O$ was not detected, except very small intensity and broad peak of $NO_2$ (supporting information) was observed over $SbV10Ce/TiO_2$ catalyst between 100 and 400 °C. This could be beneficial for the fast SCR [6] at low temperature over $SbV10Ce/TiO_2$ catalyst. In particular, the formation small crystallites of vanadia, antimony oxides and their fine dispersion on surface of $CeO_2$-$TiO_2$ improved the catalytic activity at wide temperatures. Fig. 7 (C) represents the mass spectra of $O_2$ of the three catalysts. All the three catalysts showed two peaks at the temperatures above 400 °C. These spectra clearly confirmed that the peaks observed at high temperatures in NO-TPD are corresponded to $O_2$. This may attributed to the chemisorbed oxygen, which was adsorbed during the pretreatment of the samples at 400 °C in 10% $O_2$/He and some bulk oxygen released by the $CeO_2$ or $TiO_2$.

In order to understand the $SO_2$ adsorption behavior over the synthesized catalysts, $SO_2$ TPD measurements were conducted. Fig. 8 presents the $SO_2$ TPD patterns of $SbV10Ce/TiO_2$, $V10Ce/TiO_2$ and $SbV/TiO_2$ catalysts calcined at 500 °C. There is clear synergism between the NO TPD and $SO_2$ TPD. The $SbV10Ce/TiO_2$ catalyst showed lowest $SO_2$ adsorption properties. Furthermore, the $SbV/TiO_2$ catalyst showed a low temperature shift signal at around 600 °C, which reveals the inhibition behavior of the Sb with respect to $SO_2$ adsorption. The addition of ceria to $SbV/TiO_2$ catalyst further enhanced the NO adsorption and inhibited the $SO_2$ adsorption properties. Therefore, the high $NO_x$ conversion for $SbV10Ce/TiO_2$ could be attributed to the NO adsorption and $SO_2$ inhibition properties.

The $NH_3$-TPD patterns of the synthesized catalysts are depicted in Fig. 9. All the three ($SbV/TiO_2$, $SbV10Ce/TiO_2$ and $V10Ce/TiO_2$) catalysts displayed two broad $NH_3$ desorption peaks at 120–240 °C and 250–450 °C temperatures, respectively. The ammonia desorbed at low temperatures was ascribed to weak acidic sites, which correspond to physisorbed ammonia and partially ionic $NH_4^+$ bound to Brønsted acid sites [34]. The high temperature desorbed ammonia was ascribed to desorption of coordinated $NH_3$ bound Lewis acid sites [35]. Indeed, the ammonia adsorption ability of the catalyst is generally considered as one of the most important criteria for the screening of catalytic systems for the $NH_3$-SCR [36]. As we notice from Fig. 9, the ceria promoted catalysts showed predominantly more desorbed ammonia at low as well as high temperatures. It seems that cerium species create new acidic sites suggest a progressive increase of the surface acidity owing to the addition of ceria. This is exceptionally beneficial for the enhancement of the $NO_x$ reduction activity with ammonia. The total acidity of the catalysts was calculated in mmol/$m^2$ of ammonia adsorbed on the catalysts and represented in Table 1. The drastic improvement in the total acidity was observed for $SbV10Ce/TiO_2$ catalyst compared to those of $SbV/TiO_2$ and $V10Ce/TiO_2$ catalysts. Thus, the improvement in ammonia adsorption over ceria doped catalysts is believed to be significantly beneficial to the $NO_x$ reduction by ammonia at wide range of temperatures.

To investigate the presence of reducible species in the prepared catalysts, the $H_2$-TPR experiment was carried out. Fig. 10 illustrates the $H_2$-TPR patterns for $SbV/TiO_2$, $SbV10Ce/TiO_2$ and $V10Ce/TiO_2$ catalysts. All the three catalysts showed major reduction peak between 300 to 600 °C, which could be assigned to the

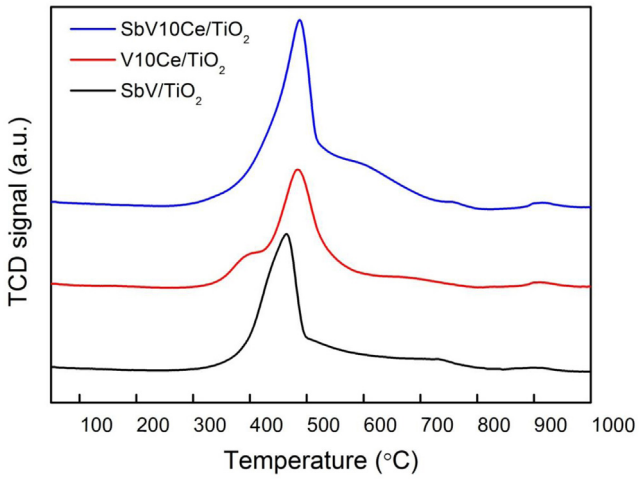


**Fig. 10.** $H_2$-TPR patterns of $SbV/TiO_2$, $SbV10Ce/TiO_2$ and $V10Ce/TiO_2$ samples.

reduction of surface antimony, vanadia and ceria species. These surface reduction peaks were attributed to the reductions from $Sb^{5+}$ to $Sb^{3+}$, $V^{5+}$ to $V^{3+}$ and $Ce^{4+}$ to $Ce^{3+}$ [37]. The values of peak maximum temperatures ($T_{max}$) along with their respective $H_2$-uptakes are represented in Table 1. The $SbV/TiO_2$ catalyst exhibited the maximum reduction peak at low temperatures around 464 °C, while the ceria added $V/TiO_2$ catalyst increased the maximum reduction peak temperature to 483 °C. This peak showed a small shoulder peak at low temperatures around 392 °C, which may be corresponded to the reduction of surface dispersed ceria species [12]. In case of ceria added $SbV/TiO_2$ catalyst, the reduction peak started from low temperatures and then the $H_2$ consumption was significantly enhanced by reaching the maximum peak at the temperature around 488 °C along with a small shoulder peak at 600 °C. This could be attributed due to the interaction between surface antimony, vanadia and ceria species. However, the amount of $H_2$ consumption for $V10Ce/TiO_2$ catalyst was less than that of $SbV/TiO_2$ and $SbV10Ce/TiO_2$. According to this result it may be suggested that the surface reduction of antimony oxides provides more lattice oxygen which is also well supported by XPS results in the later discussion. The synergistic effect of antimony, vanadia and ceria on $TiO_2$ could induce thermal stability of the $SbV10Ce/TiO_2$ catalyst and thus, increases high temperature $NO_x$ reduction activity (>350 °C). The total number of reducible species also increases for $SbV10Ce/TiO_2$ catalyst and shows highest $H_2$ consumption than $SbV/TiO_2$ and $V10Ce/TiO_2$ catalysts. In ceria added $SbV10Ce/TiO_2$ and $V10Ce/TiO_2$ catalysts a small reduction peak appeared at above 900 °C temperatures, which could be attributed to the reduction of bulk ceria. From the above results, it can be concluded that the high acidity and high reducibility of $SbV10Ce/TiO_2$ catalyst played an important role in increasing $NO_x$ conversion efficiency in a wide temperature widow.

Surface atomic concentrations of Ce, Sb, V, O and Ti from XPS are summarized in Table 2. The photoelectron spectra of Ce 3d, V 2p, O 1s and Ti 2p are displayed in Fig. 11. Table 1 shows that the atomic ratio of V/Ti over the surface of $SbV10Ce/TiO_2$ and $V10Ce/TiO_2$ are 0.07 and 0.10. They are relatively higher than that of $SbV/TiO_2$ catalyst (0.05). This result ascertained well dispersion of vanadia over the surface of $TiO_2$ support with the addition of ceria. Fig. 11(A) displays two main characteristic peaks observed at 901.0 and 883.0 eV binding energy, which corresponding to Ce ($3d_{3/2}$) and Ce ($3d_{5/2}$), respectively. These two ($3d_{3/2}$ and $3d_{5/2}$) broad peaks attributed to the mixed valance cerium oxidation ($Ce^{4+}$ and $Ce^{3+}$ species) states over the surface of $V10Ce/TiO_2$ and $SbV10Ce/TiO_2$ catalysts [38]. The XPS spectra of Ce 3d peaks are denoted as v, v″ and u, u″ assigned to $Ce^{4+}$ species while v′, u′ are assigned to $Ce^{3+}$ species [39]. The binding energy of v′ peak belonging to $Ce^{3+}$ for $V10Ce/TiO_2$ and $SbV10Ce/TiO_2$ catalysts appeared at 885.6 and 885.8 eV. These $Ce^{3+}$ species could create a charge imbalance vacancies and unsaturated chemical bonds on the catalyst surface, which could lead to the increase of chemisorbed oxygen on the surface of the catalysts.

Fig. 11(B) shows XPS spectra of V 2p of the three catalysts $SbV/TiO_2$, $V10Ce/TiO_2$ and $SbV10Ce/TiO_2$. The center of the peak binding energy of V $2p_{3/2}$ of the three catalysts exists at 516.8 eV. According to the handbook of the elements and native oxides for XPS [40], the reported V $2p_{3/2}$ peak binding energies for the oxidation state of $V^{5+}$ is in the range from 517.4 to 516.4 eV and the oxidation state of $V^{4+}$ lies in the range of 515.7 to 515.4 eV. It is observed that the $SbV/TiO_2$ catalyst shows the $V^{5+}$ peak binding energy at 516.5 eV, whereas the ceria loaded $SbV10Ce/TiO_2$ and $V10Ce/TiO_2$ catalysts showed the slightly shift in binding energies toward high at 516.7 and 516.9 eV. The existence of V $2p_{3/2}$ peak between 518.4–515.0 eV on the surface of $SbV10Ce/TiO_2$ catalyst indicates the coexistence of $V^{5+}$ and $V^{4+}$ species [41,42]. This would favor the catalytic reaction of $NH_3$-SCR over $SbV10Ce/TiO_2$ catalyst and eventually leads to higher $NO_x$ conversions at wide range of temperatures.

The XPS spectra of O 1s peak (Fig. 11(C)) could be fitted into two peaks. The peak appeared at lower binding energy (530.3–529.2 eV) could be assigned to the lattice oxygen ($O_\beta$) and additional peak appeared at higher binding energy (532.5–531.5 eV) is corresponded to the surface chemisorbed oxygen ($O_\alpha$) [43]. The surface chemisorbed oxygen ($O_\alpha$) has been reported to be the most active oxygen in the oxidation reactions due to its higher mobility than the lattice oxygen ($O_\beta$) [10,44]. It can be clearly observed from Table 1 that the addition of ceria increased the percentage of $O_\alpha$ over the surface of $SbV10Ce/TiO_2$ and $V10Ce/TiO_2$ compared to that of $SbV/TiO_2$ catalyst. On the other hand, the peak intensity of $O_\beta$ is very high in $SbV10Ce/TiO_2$ and $SbV/TiO_2$ catalysts than $V10Ce/TiO_2$, which is very clear from the Fig. 11(C). This could be due to the presence of antimony. Therefore, the above results indicate that the addition of ceria promoted the formation of fairly higher amount of surface chemisorbed mobile oxygen ($O_\alpha$) and lattice oxygen ($O_\beta$) species. Consequently, higher $NO_x$ conversion in $SbV10Ce/TiO_2$ catalyst over wide temperature range was observed.

Fig. 11(D) displays the XPS spectra of Ti 2p of the three catalysts. The peaks corresponding to Ti $2p_{1/2}$ and $2p_{3/2}$ for $SbV/TiO_2$ catalyst are observed at binding energies 464.6 and 458.8 eV, respectively. This indicates that Ti exists in $Ti^{4+}$ oxidation state [43] and they are observed at slightly smaller binding energies than that of pure $TiO_2$ (the binding energies of Ti $2p_{1/2}$ and $2p_{3/2}$ peaks are observed at 464.7 and 458.9 eV, respectively). This might be due to the fact that stronger affinity of electron cloud by $Ti^{4+}$. Addition of ceria leads to an enhancement in the electron affinity of Ti and causes lower binding energies for $V10Ce/TiO_2$ (Ti $2p_{1/2}$ and $2p_{3/2}$ – 464.3 and 458.5 eV) and $SbV10Ce/TiO_2$ (Ti $2p_{1/2}$ and $2p_{3/2}$ – 464.2 and 458.4 eV) catalysts. These results reveal that ceria has strong interaction with the surface of the $TiO_2$ and influence the catalytic activity of the catalyst. It is also observed that the shift in binding energy of the Ti 2p spectra toward lower binding energy follows the sequence: $SbV/TiO_2 > V10Ce/TiO_2 > SbV10Ce/TiO_2$. This low binding energy shift of Ti 2p ($SbV10Ce/TiO_2$) peak is mainly due to interaction of antimony, vanadia and ceria on the surface of well defined $TiO_2$.

The TEM images and EDS spectra of fresh and used $SbV10Ce/TiO_2$ catalysts are depicted in Fig. 12(A) and (B). The morphology of these oxides seems to be configured by a stack of spherical particles. Both

**Table 2**
XPS results of various samples calcined at 500 °C.

| S. No. | Catalyst | Surface atomic concentration (%) | | | | | | | | |
|---|---|---|---|---|---|---|---|---|---|---|
| | | Ti | V | Sb | Ce | O | | | V/Ti | Ce/Ti |
| | | | | | | [a]$O_T$ | [b]$O_\alpha$ | [b]$O_\beta$ | | |
| 1 | $SbV/TiO_2$ | 20.99 | 1.06 | 1.07 | – | 76.87 | 8.3 | 91.7 | 0.05 | – |
| 2 | $SbV10Ce/TiO_2$ | 17.45 | 1.19 | 1.06 | 1.29 | 79.01 | 13.5 | 86.5 | 0.07 | 0.06 |
| 3 | $V10Ce/TiO_2$ | 20.83 | 2.14 | – | 0.94 | 76.01 | 39.5 | 60.5 | 0.10 | 0.04 |

[a] Atomic concentration of the total oxygen.
[b] Percentage of peak area of $O_\alpha$ and $O_\beta$.

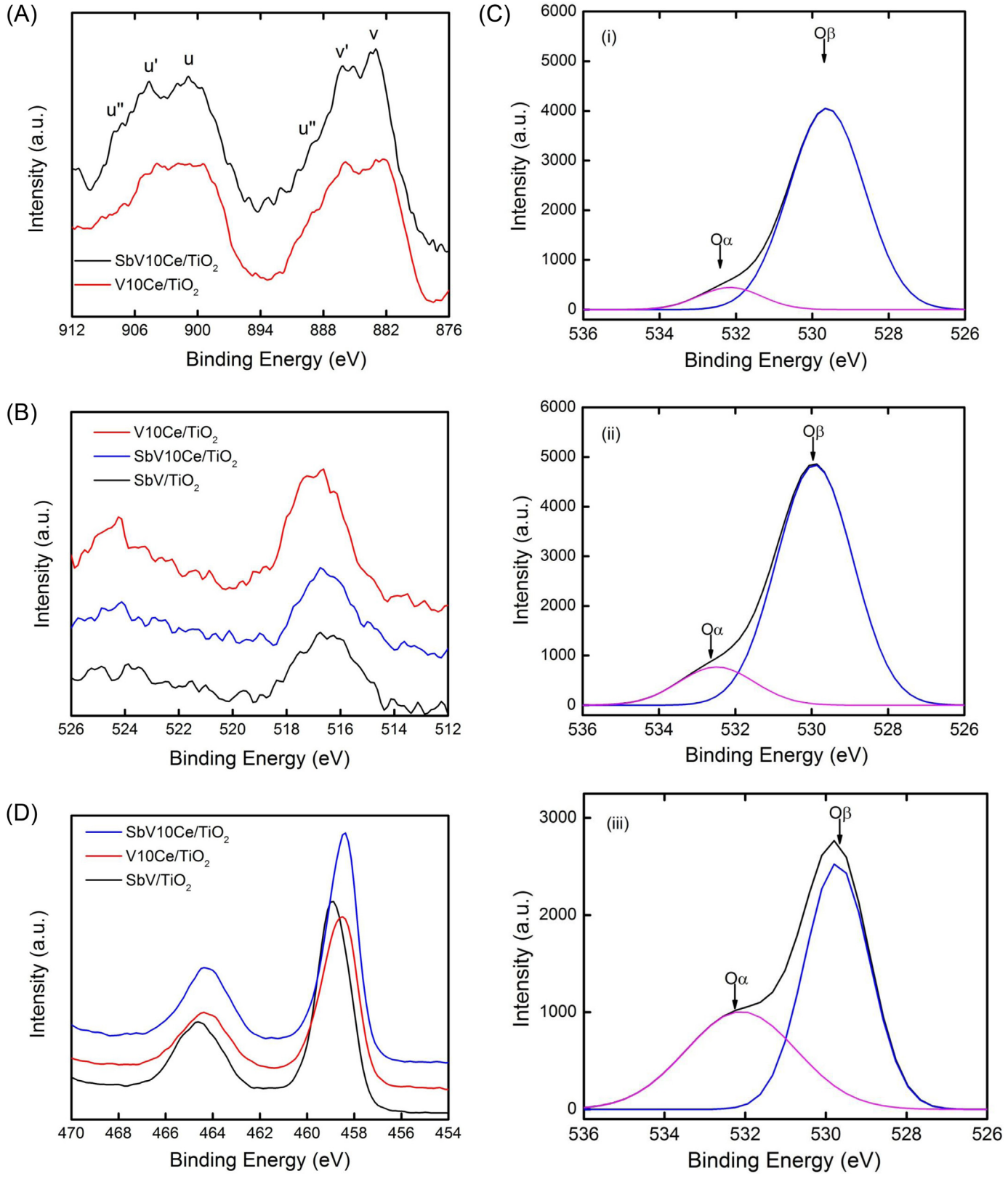


**Fig. 11.** XPS spectra of (A) Ce 3d of $SbV10Ce/TiO_2$ and $V10Ce/TiO_2$, (B) V 2p of $SbV/TiO_2$, $SbV10Ce/TiO_2$ and $V10Ce/TiO_2$, (C) O 1s of (i) $SbV/TiO_2$, (ii) $SbV10Ce/TiO_2$ and (iii) $V10Ce/TiO_2$, and (D) Ti 2p of $SbV/TiO_2$, $SbV10Ce/TiO_2$ and $V10Ce/TiO_2$.

fresh and used catalysts reveal a homogeneous distribution of crystallites all over the catalyst surface. Many randomly oriented groups of nano-crystallites are observed. The mean crystallite size of the fresh and used catalysts is ~25 nm, indicating no sintering effect at higher temperatures under the reaction conditions. The EDS spectra of the fresh and used catalysts showed the elemental concentration of all the components. It was observed that the used catalysts had small amount of sulfur content. This could be due to the small

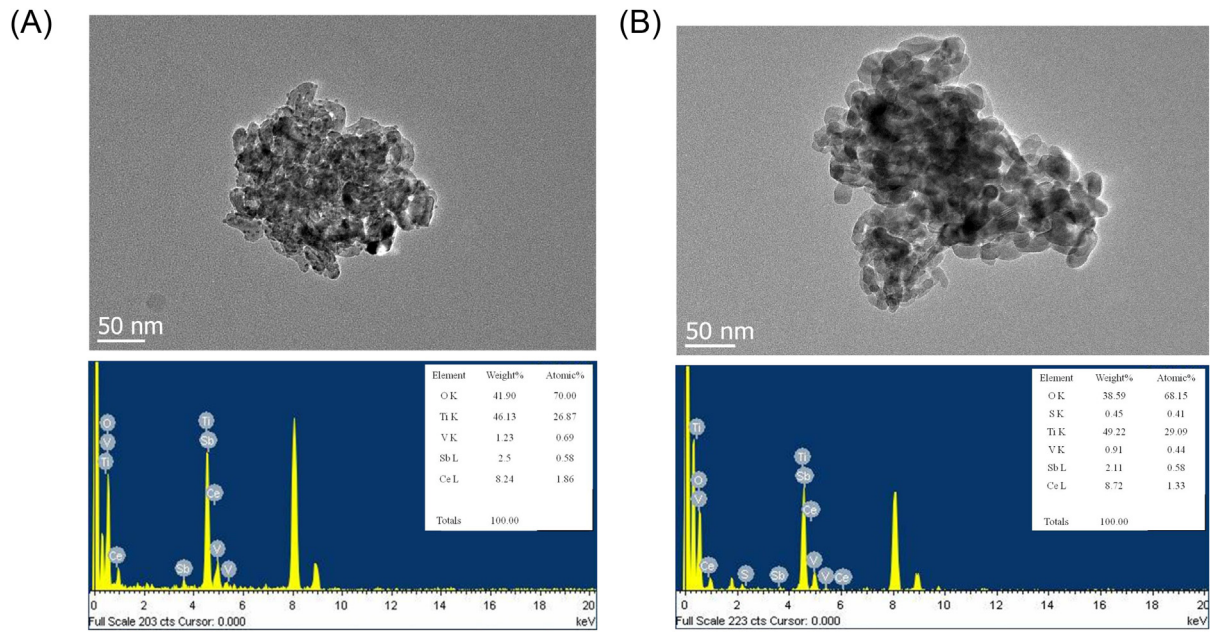


**Fig. 12.** TEM-EDS images of $SbV10Ce/TiO_2$ fresh (A) and used (B) samples.

amounts of sulfates formed in the used catalysts, which could not be able to detectable by XRD.

### 3.3. DRIFTS study

#### 3.3.1. Ammonia adsorption

The $NH_3$ desorbed at low temperatures during $NH_3$-TPD was considered to exist on Brønsted acid sites and that desorbed at high temperature was considered to exist on Lewis acid sites. However, $NH_3$-TPD cannot differentiate the Brønsted acid sites and Lewis acid sites i.e., the weak acid sites may contain few Lewis acid sites and the strong acid sites may contain Brønsted acid sites. Therefore, it was necessary to investigate the Brønsted and Lewis acid sites through DRIFT spectroscopy. The catalysts were subjected to DRIFTS analysis with ammonia adsorption at room temperature and the resultant desorption spectra are shown in Fig. 13 at different temperatures (50, 150, 250 and 350 °C). Fig. 13(A) represents the DRIFT spectra of $NH_3$ adsorption on $SbV10Ce/TiO_2$ catalyst at 50, 150, 250 and 350 °C temperatures. The vibration of N-H deformation band of adsorbed ammonia molecule was observed in the range of 1100–1700 $cm^{-1}$. It is an important fingerprint region to differentiate the Lewis and Brønsted acid sites [45–47]. The bands observed at 1257 and 1603 $cm^{-1}$ can be assigned to asymmetric and symmetric bending vibrations of the N—H bonds in $NH_3$ coordinately linked to Lewis acid sites [46], while the bands at 1436 and 1673 $cm^{-1}$ could be assigned to asymmetric and symmetric bending vibrations of $NH_4^+$ bound to Brønsted acid sites [46,47]. It is noteworthy that the $NH_3$ adsorbed on Brønsted acid sites was much higher than that of Lewis acid sites.

Fig. 13(B) indicates the DRIFT spectra of $NH_3$ adsorption on $V10Ce/TiO_2$ catalyst, which is similar to that of $SbV10Ce/TiO_2$ catalyst except that the bands at 1436 and 1603 $cm^{-1}$ were slightly shifted to 1440 and 1601 $cm^{-1}$, respectively. However, the bands of Brønsted and Lewis acid sites were almost disappeared above 150 °C over $V10Ce/TiO_2$, while the $SbV10Ce/TiO_2$ catalyst shows decrease in intensity of Brønsted and Lewis acid sites until 250 °C temperature. This confirms that $SbV10Ce/TiO_2$ catalyst possesses abundant Brønsted and Lewis acid sites than $V10Ce/TiO_2$ catalyst. The catalyst without ceria ($SbV/TiO_2$) shows the less Brønsted acid sites and more Lewis acid sites compared to $SbV10Ce/TiO_2$ and $V10Ce/TiO_2$ catalysts (Fig. 13(C)). These Lewis acid and Brønsted acid sites are observed at 1240, 1600 $cm^{-1}$ bands and 1463, 1673 $cm^{-1}$ bands, respectively on $SbV/TiO_2$ catalyst. However, the peaks corresponding to Brønsted acid and Lewis acid sites were disappeared above 150 °C temperatures on $SbV/TiO_2$ catalyst. According to the literature and our experimental results, the presence of abundant Brønsted acid sites on $SbV10Ce/TiO_2$ catalyst should be responsible for the increase of the SCR activities at wide range of temperatures [48]. It was interesting to note that a weak peak at 1562 $cm^{-1}$ appeared in DRIFT spectra for $SbV10Ce/TiO_2$ and $V10Ce/TiO_2$ catalysts. This peak is attributed to the $—NH_3^+$ group [49], which indicating that the $—NH_3^+$ might have formed from the decomposition of $NH_4^+$ adsorbed on the Brønsted acid sites. Especially, a group of peaks at 1330–1380 $cm^{-1}$ were observed on $SbV/TiO_2$ catalyst, which could be assigned to the intermediates of ammonia oxidation species and their intensities increases drastically on $SbV/TiO_2$ catalyst above 250 °C. This indicates that the direct oxidation of ammonia is provoked at higher temperatures over $SbV/TiO_2$, which leads to lower $NO_x$ conversions for $SbV/TiO_2$ catalyst than ceria loaded catalysts above 350 °C temperatures.

#### 3.3.2. Reaction between nitrogen oxides and ammonia pre-adsorbed species

The DRIFTS experimental results of $NH_3$ adsorption followed by Nitric oxides reaction with Lewis and Brønsted acid sites on surface of the $SbV10Ce/TiO_2$ and $SbV/TiO_2$ catalysts were displayed in Fig. 14(A) and (B). The catalysts were pre-adsorbed with 800 ppm ammonia for 30 min at 200 °C, followed by $N_2$ purging. 800 ppm NO + 3 vol% $O_2$ was then introduced into the DRIFTS cell at 200 °C, and the spectra were recorded as a function of time. As we noted already, the bands assigned to $NH_3$ species coordinately linked to Lewis acid sites and $NH_4^+$ bound to Brønsted acid sites were observed at 1591 $cm^{-1}$ and 1433 $cm^{-1}$ on $SbV10Ce/TiO_2$ catalyst upon treatment with $NH_3$. The bands attributed to Lewis and Brønsted acid sites were quickly vanished over $SbV10Ce/TiO_2$ (Fig. 14(A)) after the introduction of NO + $O_2$. At the same time, several new bands were observed at 1613, 1588 and 1558 $cm^{-1}$, which corresponded to the intermediate species of $NO_x$. The band

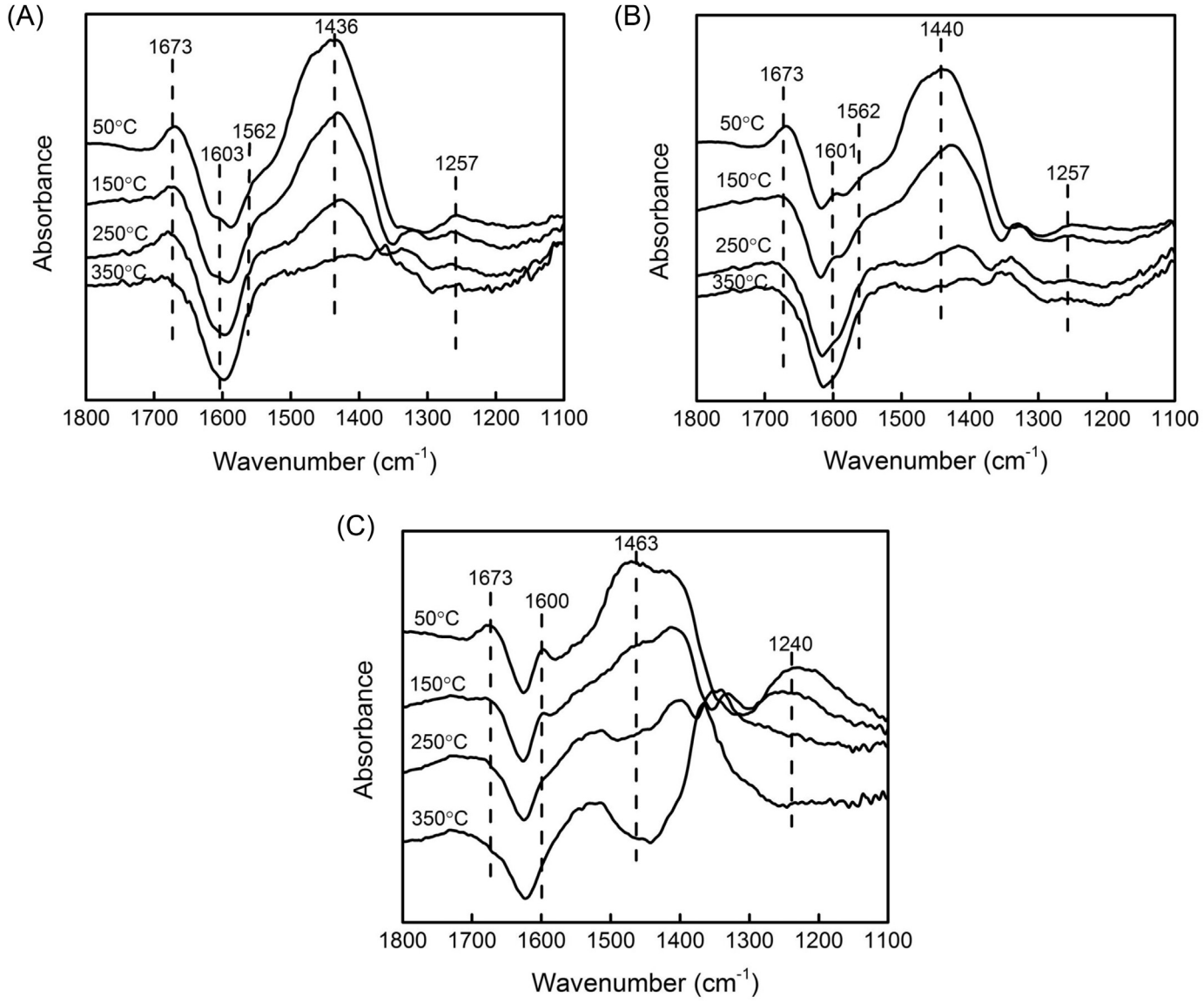


**Fig. 13.** DRIFTS spectra of (A) SbV10Ce/$TiO_2$ (B) V10Ce/$TiO_2$ and (C) SbV/$TiO_2$ exposed to 2000 ppm $NH_3$ for 30 min at room temperature and then purged by $N_2$ at 50, 150, 250 and 350 °C.

at 1613 $cm^{-1}$ may be attributed to the $NO_2$ species [50]. The bands at 1588 and 1558 $cm^{-1}$ were attributed to the nitrite and nitrate ($NO_2^-$ and $NO_3^-$) species [51]. In case of SbV/$TiO_2$ catalyst, the spectrum obtained after the adsorption of ammonia was relatively similar, except that the intensity of the band assigned to Brønsted acid sites was less than that of SbV10Ce/$TiO_2$ catalyst. Also, the bands attributed to Lewis and Brønsted acid sites were slightly shifted to 1597 and 1463 $cm^{-1}$ (Fig. 14(B)). The formation of intermediate $NO_x$ species was observed over SbV/$TiO_2$ catalyst, after the introduction of NO + $O_2$ on $NH_3$ presorbed catalyst surface at 1603 and 1568 $cm^{-1}$. These bands were attributed to the nitrite and nitrate species. But, the formation of $NO_2$ species was not observed on SbV/$TiO_2$ catalyst. This means that the addition of ceria to SbV/$TiO_2$ catalyst promoted the formation of $NO_2$ at low temperatures (200 °C) and it is beneficial for the fast SCR. Koebel et al. investigated the low temperature fast SCR behavior on $V_2O_5$/$TiO_2$ based catalysts [52,53], which is well supported with our in situ DRIFTS results. The negative peak at 2030 $cm^{-1}$ was due to the overtone of V=O on SbV10Ce/$TiO_2$ and SbV/$TiO_2$ catalysts. These negative peaks indicate that V=O groups on the catalyst surface are consumed upon ammonia absorption [54]. The adsorbed ammonia reacted with NO as a function of time and then decreased the intensity of the negative peak of V=O in both the catalysts.

### 3.4. $SO_2$ on–off study

The exhaust gas usually contains both $H_2O$ and $SO_2$, which are likely to poison the catalysts and then decreases the $NO_x$ conversion. Therefore, $H_2O$ and $SO_2$ tolerance of SbV/$TiO_2$, SbV10Ce/$TiO_2$ and V10Ce/$TiO_2$ catalysts, and their long-term durability studies with $SO_2$ on–off cycles were performed under isothermal conditions at 240 °C. As illustrated in Fig. 15, when 6 vol% $H_2O$ and 800 ppm $SO_2$ are simultaneously added to the gas reaction mixture, the $NO_x$ removal efficiency declined at different rates for the three catalytic systems. A gradual decrease in every 5 h during $SO_2$ on–off cycle for the following 38 h of continuous run was observed. Among all the catalysts, SbV10Ce/$TiO_2$ catalyst underwent small decrease in $NO_x$ conversion from 98% to 91%. However, the $NO_x$ conversion of V10Ce/$TiO_2$ and SbV/$TiO_2$ catalysts was decreased significantly from 91% to 75% and 93% to 60%, respectively. These results express a clear difference in deactivation behavior of the catalysts due to poisoning effect of $H_2O$ and $SO_2$. In the presence

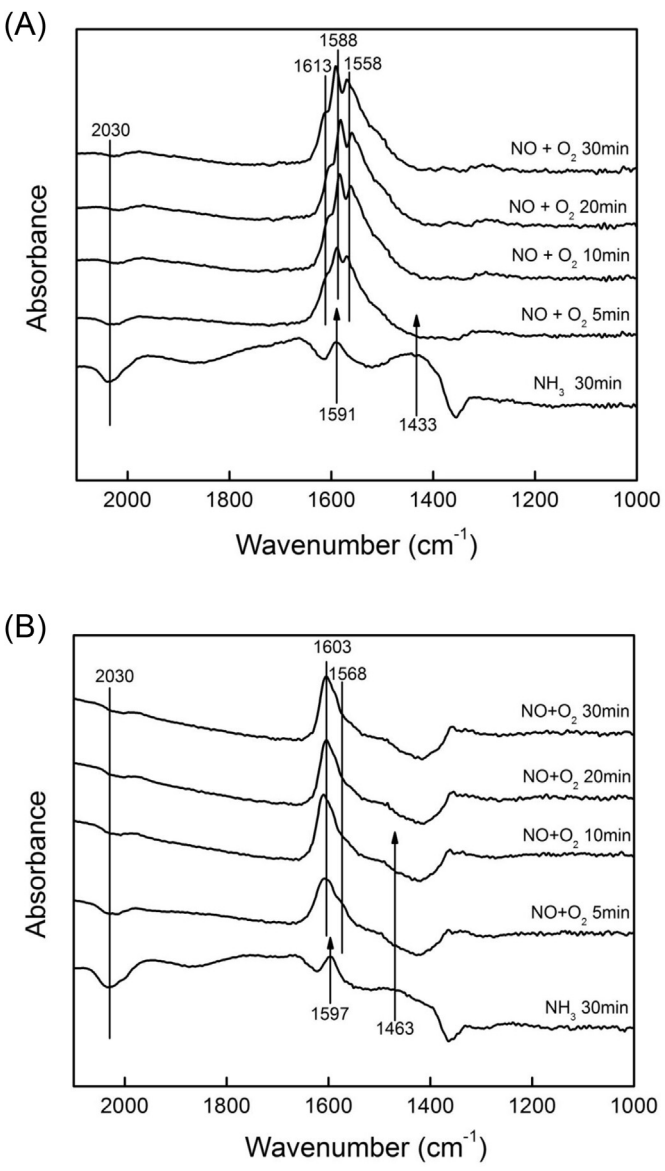


**Fig. 14.** DRIFTS spectra of (A) $SbV10Ce/TiO_2$ and (B) $SbV/TiO_2$ catalysts exposed to 800 ppm $NH_3$ for 30 min at 200 °C, followed by $N_2$ purging and then exposed to 800 ppm NO + 3 vol% $O_2$ as a function of time.

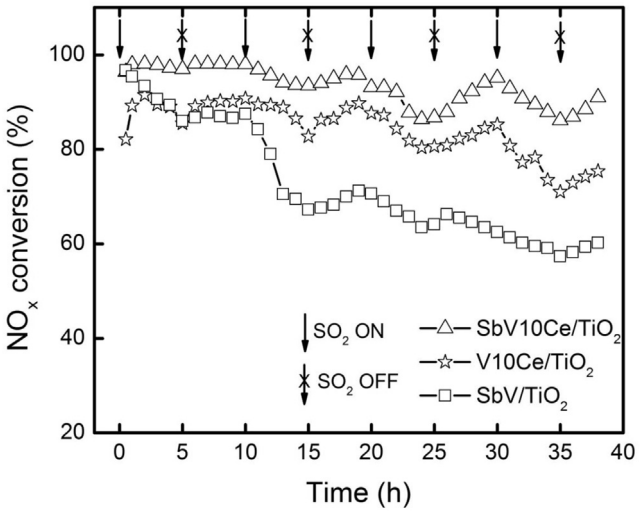


**Fig. 15.** $SO_2$ on–off studies on $SbV10Ce/TiO_2$, $V10Ce/TiO_2$ and $SbV/TiO_2$ samples: With $SO_2$ and $H_2O$ at 240 °C. (Reaction Conditions: $[NO_x] = [NH_3] = 800$ ppm, $[O_2] = 3$ vol%, $H_2O = 6$ vol%, $SO_2 = 800$ ppm, $N_2$ balance, GHSV = 60,000 $h^{-1}$).

of $SO_2$ and $H_2O$, $SO_2$ can be oxidized to $SO_3$ by $O_2$ and these $SO_x$ ($SO_2 + SO_3$) compounds eventually forms ammonium sulfate ($(NH_4)_2SO_4$) or ammonium bisulfate ($NH_4HSO_4$) by reacting with slipped $NH_3$ and $H_2O$ [27,55]. It could be possible that the formation of ammonium sulfate ($(NH_4)_2SO_4$) or ammonium bisulfate ($NH_4HSO_4$) species over $SbV/TiO_2$ and $V10Ce/TiO_2$ catalysts occur faster than over $SbV10Ce/TiO_2$. This might result in blocking of the catalytic pores and occupying the catalytic active sites. Conversely, the $SbV10Ce/TiO_2$ catalyst showed higher resistance to $SO_2$ and water during 38 h of continuous study. During the course of the reaction over $SbV10Ce/TiO_2$ catalyst, the small amount of formed ammonium sulfates are removed by water in the absence of $SO_2$ ($SO_2$ off cycle) and then showed gradual increment in the $NO_x$ conversion efficiency. On the other hand, the amounts of ammonium sulfates formed over $SbV/TiO_2$ and $V10Ce/TiO_2$ catalysts are more, which are not removed completely by water in the absence of $SO_2$, leading to continuous deactivation of those catalysts. The results of $SO_2$-TPD for $SbV10Ce/TiO_2$ catalyst are in good agreement with these results, where less $SO_2$ adsorption gave a hint to its strong resistance toward $SO_2$ and lower probability of ultimate salts formation. Consequently, $SbV10Ce/TiO_2$ catalyst increases resistance against $SO_2$ and $H_2O$ during $SO_2$ on–off long term stability under isothermal conditions at 240 °C temperature for 38 h.

## 4. Conclusions

The various ceria loaded $Sb\text{-}V_2O_5/TiO_2$ catalysts were developed for the reduction of $NO_x$ with $NH_3$, especially in the temperature region between 180-500 °C. The addition of 10% ceria to $Sb\text{-}V_2O_5/TiO_2$ catalyst showed excellent $NO_x$ conversion with higher than 87% in a wide temperature window of 220–500 °C. This catalyst exhibits superior $N_2$ selectivity than $Sb\text{-}V_2O_5/TiO_2$ and $V_2O_5\text{-}10Ce/TiO_2$ catalyst. The 10% ceria loaded $Sb\text{-}V_2O_5/TiO_2$ catalyst also exhibits strong resistance to 6% $H_2O$ and 800 ppm $SO_2$ at low temperatures around 220 °C and possesses high $NO_x$ conversion (90%) and $N_2$ selectivity (100%).

The $NH_3$-TPD and NO-TPD results for $Sb\text{-}V_2O_5\text{-}10Ce/TiO_2$ catalyst show high acidity and high NO adsorption ability, which could be responsible for the high $NO_x$ conversions at wide range of temperatures. $H_2$-TPR reveals a strong interaction between antimony, vanadia and ceria, which resulted in increased $H_2$ uptakes and high temperature reduction peak. The XRD results for the fresh and used catalysts of 10% ceria loaded $Sb\text{-}V_2O_5/TiO_2$ showed no change in their spectra and was well supported by TEM images, which demonstrates the high compositional stability and mechanical strength of the prepared catalysts even in the presence of excess $H_2O$ and $SO_2$. Furthermore, results of XPS revealed the presence of $Ce^{4+}/Ce^{3+}$ species could increase chemisorbed oxygen over ceria added catalysts.

The DRIFT spectra of $Sb\text{-}V_2O_5\text{-}10Ce/TiO_2$ catalyst showed Brønsted acid sites at 1436 and 1673 $cm^{-1}$ band until 250 °C temperature, which suggested the presence of abundant Brønsted acid sites on $Sb\text{-}V_2O_5\text{-}10Ce/TiO_2$ compared to $Sb\text{-}V_2O_5/TiO_2$ and $V_2O_5\text{-}10Ce/TiO_2$ catalysts. This contributed to the high $NH_3$-SCR activity for $Sb\text{-}V_2O_5\text{-}10Ce/TiO_2$ catalyst at wide temperature window. $SO_2$-TPD and NO-TPD results revealed that $Sb\text{-}V_2O_5\text{-}10Ce/TiO_2$ catalyst significantly enhanced the NO adsorption and $SO_2$ inhibition properties which guided to high activity and selectivity at wide temperatures and exhibits high $H_2O$ and $SO_2$ tolerance during 38 h under isothermal conditions at 240 °C.

## Acknowledgements

This work was financially supported by 'Future Core Technology' program from KIST and a grant from the Fundamental R&D Program for the core technology of materials, funded by the Ministry of Knowledge Economy of the Republic of Korea.

## Appendix A. Supplementary data

Supplementary data associated with this article can be found, in the online version, at http://dx.doi.org/10.1016/j.apcatb.2013.05.071.

## References

[1] H. Bosch, F. Janssen, Catal. Today 2 (1988) 369–379.
[2] K.C. Taylor, Catal. Rev. Sci. Eng. 35 (1993) 457–481.
[3] G. Madia, M. Elsener, M. Koebel, F. Raimondi, A. Wokaun, Appl. Catal. B 39 (2002) 181–190.
[4] C. Ciardelli, I. Nova, E. Tronconi, D. Chatterjee, B. Bandl-Konrad, M. Weibel, B. Krutzsch, Appl. Catal. B 70 (2007) 80–90.
[5] M. Koebel, M. Elsener, M. Kleemann, Catal. Today 59 (2000) 335–345.
[6] I. Nova, C. Ciardelli, E. Tronconi, D. Chatterjee, B. Bandl-Konrad, Catal. Today 114 (2006) 3–12.
[7] Y.J. Kim, H.J. Kwon, I-S. Nam, J.W. Choung, J.K. Kil, H-J. Kim, M-S. Cha, G.K. Yeo, Catal. Today 151 (2010) 244–250.
[8] F. Kapteijn, L. Singoredjo, M. Vandriel, A. Andreini, J.A. Moulijn, G. Ramis, G. Busca, J. Catal. 150 (1994) 105–116.
[9] P.G. Smirniotis, D.A. Peña, B.S. Uphade, Angew. Chem. Int. Ed. 40 (2001) 2479–2482.
[10] G. Carja, Y. Kameshima, K. Okada, C.D. Madhusoodana, Appl. Catal. B 73 (2007) 60–64.
[11] S. Roy, B. Viswanath, M.S. Hegde, G. Madras, J. Phys. Chem. C 112 (2008) 6002–6012.
[12] L. Chen, J. Li, M. Ge, J. Phys. Chem. C 113 (2009) 21177–21184.
[13] H. Suzuki, M. Riemi, T. Naoki, Toyota Tech. Rev. 46 (1996) 68–81.
[14] S. Matsumoto, Y. Ikeda, H. Suzuki, M. Ogai, N. Miyoshi, Appl. Catal. B 25 (2000) 115–124.
[15] A. Trovarelli, G. Dolcetti, C. de Leitenburg, J. Kaspar, P. Finetti, A. Santoni, J. Chem. Soc., Faraday Trans. 88 (1992) 1311–1319.
[16] C. Serre, F. Garin, G. Belot, G. Marie, J. Catal. 141 (1993) 9–20.
[17] M.F.M. Zwinkels, S.G. Jaras, P.G. Menon, T.A. Griffin, Catal. Rev. Sci. Eng. 35 (1993) 319–358.
[18] B. Murugan, A.V. Ramaswamy, J. Am. Chem. Soc. 129 (2007) 3062–3063.
[19] C.T. Campbell, C.H.F. Peden, Science 309 (2005) 713–714.
[20] G. Busca, L. Lietti, G. Ramis, F. Berti, Appl. Catal. B 18 (1998) 1–36.
[21] R.Q. Long, R.T. Yang, R. Chang, Chem. Commun. 5 (2002) 452–453.
[22] H.H. Phil, M.P. Reddy, P.A. Kumar, L.K. Ju, J.S. Hyo, Appl. Catal. B 78 (2008) 301–308.
[23] K.N. Rao, B.M. Reddy, S-E. Park, Appl. Catal. B 100 (2010) 472–480.
[24] T. Kim, I.E. Wachs, J. Catal. 255 (2008) 197–205.
[25] L. Lietti, I. Nova, G. Ramis, L.Dall'Acqua, G. Busca, E. Giamello, P. Forzatti, F. Bregani, J. Catal. 187 (1999) 419–435.
[26] L. Chen, J. Li, M. Ge, R. Zhu, Catal. Today 153 (2010) 77–83.
[27] J. Huang, Z. Tong, Y. Huang, J. Zhang, Appl. Catal. B 78 (2008) 309–314.
[28] S. Solomon, D. Qin, M. Manning, Z. Chen, M. Marquis, K.B. Averyt, M. Tignor, H.L. Miller, Climate Change 2007: The Physical Science Basis, Cambridge, UK and New York, NY, 2007.
[29] F.D. Liu, H. He, J. Phys. Chem. C 114 (2010) 16929–16936.
[30] F.D. Liu, H. He, Y. Ding, C.B. Zhang, Appl. Catal. B 93 (2009) 194–204.
[31] H-B. Chiang, M-D. Lee, Appl. Catal. A 154 (1997) 55–74.
[32] H. Zou, Y.S. Lin, Appl. Catal. A 265 (2004) 35–42.
[33] P. Afanasiev, Catal. Commun. 9 (2008) 734–739.
[34] S. Roy, M.S. Hedge, G. Madras, Appl. Energy 86 (2009) 2283–2297.
[35] L. Chmielarz, R. Dziembaj, T. Grzybek, J. Klinik, T. Lojewski, D. Olszewska, A. Wegrzyn, Catal. Lett. 70 (2000) 51–56.
[36] E-Y. Choi, I-S. Nam, Y.G. Kim, J. Catal. 161 (1996) 597–604.
[37] S. Besselmann, C. Freitag, O. Hinrichsen, M. Muhler, Phys. Chem. Chem. Phys. 3 (2001) 4633–4638.
[38] B.M. Reddy, A. Khan, Y. Yamada, T. Kobayashi, S. Loridant, J.C. Volta, J. Phys. Chem. B 106 (2002) 10964–10972.
[39] H. He, H.X. Dai, C.T. Au, Catal. Today 90 (2004) 245–254.
[40] B. Vincent Crist, Handbook of the Elements and Native oxides, XPS, International, Inc, Mountain View, CA, 1999.
[41] M. Machida, D. Kurogi, T. Kijima, Chem. Mater. 12 (2000) 3165–3170.
[42] S. Yang, W. Zhu, Z. Jiang, Z. Chen, J. Wang, Appl. Surf. Sci. 252 (2006) 8499–8505.
[43] B. Guan, H. Lin, L. Zhu, Z. Huang, J. Phys. Chem. C 115 (2011) 12850–12863.
[44] M. Kang, E.D. Park, J.M. Kim, J.E. Yie, Appl. Catal. A 327 (2007) 261–269.
[45] N. Naito, N. Katada, M. Niwa, J. Phys. Chem. B 103 (1999) 7206–7213.
[46] A. Gutierrez-Alejandre, J. Ramirez, G. Busca, Langmuir 14 (1998) 630–639.
[47] M.A. Larrubia, G. Ramis, G. Busca, Appl. Catal. B 27 (2000) L145–L151.
[48] M.D. Amiridis, R.V. Duevel, I.E. Wachs, Appl. Catal. B 20 (1999) 111–122.
[49] J.M.G. Amores, V.S. Escribano, G. Ramis, G. Busca, Appl. Catal. B 13 (1997) 45–58.
[50] G. Qi, R.T. Yang, J. Phys. Chem. B 108 (2004) 15738–15747.
[51] H.E. Curry-Hyde, H. Musch, A. Baiker, M. Schraml-Marth, A. Wokaun, J. Catal. 133 (1992) 397–414.
[52] M. Koebel, M. Elsener, G. Madia, Ind. Eng. Chem. Res. 40 (2001) 52–59.
[53] M. Koebel, G. Madia, F. Raimondi, A. Wokaun, J. Catal. 209 (2002) 159–165.
[54] M.A.L. Vargas, M. Casanova, A. Trovarelli, G. Busca, Appl. Catal. B 75 (2007) 303–311.
[55] Z. Zhu, Z. Liu, S. Liu, H. Niu, Appl. Catal. B 30 (2001) 267–276.